Title

Resting and Task-Modulated High-Frequency Brain Rhythms Measured by Scalp Encephalography in Infants with Tuberous Sclerosis Complex

Journal

Journal of Autism and Developmental Disorders, 45(2)

ISSN

0162-3257

Authors

Stamoulis, Catherine
Vogel-Farley, Vanessa
Degregorio, Geneva
et al.

Publication Date

2015-02-01

DOI

10.1007/s10803-013-1887-7

Peer reviewed

J Autism Dev Disord
DOI 10.1007/s10803-013-1887-7

ORIGINAL PAPER

Resting and Task-Modulated High-Frequency Brain Rhythms Measured by Scalp Encephalography in Infants with Tuberous Sclerosis Complex

Catherine Stamoulis · Vanessa Vogel-Farley · Geneva Degregorio · Shafali S. Jeste · Charles A. Nelson

Abstract The electrophysiological correlates of cognitive deficits in tuberous sclerosis complex (TSC) are not well understood, and modulations of neural dynamics by neuroanatomical abnormalities that characterize the disorder remain elusive. Neural oscillations (rhythms) are a fundamental aspect of brain function, and have dominant frequencies in a wide frequency range. The spatio-temporal dynamics of these frequencies in TSC are currently unknown. Using a novel signal decomposition approach this study investigated dominant cortical frequencies in 10 infants with TSC, in the age range 18–30 months, and 12 age-matched healthy controls. Distinct spectral characteristics were estimated in the two groups. High-frequency [in the high-gamma (>50 Hz) and ripple (>80 Hz) ranges], non-random EEG components were identified in both TSC and healthy infants at 18 months. Additional components in the lower gamma (30–50 Hz) ranges were also identified, with higher characteristic frequencies in TSC than in controls. Lower frequencies were statistically identical in both sub-groups. A significant shift in the high-frequency spectral content of the EEG was observed as a function of age, independently of task performance, possibly reflecting an overall maturation of developing neural circuits. This shift occurred earlier in healthy infants than in TSC, i.e., by age 20 months the highest dominant frequencies were in the high gamma range, whereas in TSC dominant frequencies above 100 Hz were still measurable. At age 28–30 months a statistically significant decrease in dominant high frequencies was observed in both TSC and healthy infants, possibly reflecting increased myelination and neuronal connection strengthening with age. Although based on small samples, and thus preliminary, the findings in this study suggest that dominant cortical rhythms, a fundamental aspect of neurodynamics, may be affected in TSC, possibly leading to impaired information processing in the brain.

Keywords Tuberous sclerosis complex · Brain dynamics · EEG · Dominant brain rhythms

C. Stamoulis (✉)
Departments of Radiology and Neurology and Clinical Research Center, Boston Children's Hospital, 300 Longwood Ave., Boston, MA 02115, USA
e-mail: caterina.stamoulis@childrens.harvard.edu

C. Stamoulis · C. A. Nelson
Harvard Medical School, Boston, MA, USA

V. Vogel-Farley · G. Degregorio · C. A. Nelson
Division of Developmental Medicine, Boston Children's Hospital, 300 Longwood Ave., Boston, MA 02115, USA

V. Vogel-Farley · G. Degregorio · C. A. Nelson
Laboratories of Cognitive Neuroscience, 1 Autumn St, Boston, MA 02115, USA

S. S. Jeste
Center for Autism Research and Treatment, Semel Institute, University of California, Los Angeles, Los Angeles, CA, USA

Introduction

Tuberous sclerosis complex (TSC) is a rare autosomal dominant disorder that affects 1 in 6,000 births (Webb et al. 1991). The syndrome is characterized by benign tumors (hamartomas) in the heart (rhabdomyomas), kidneys (angiomyolipomas), skin and brain (cortical tubers and subependymal nodules and astrocytomas). TSC is caused by mutations in either the TSC1 or TSC2 genes (Kandt et al. 1992; Van et al. 1997), with potentially more severe effects in patients with TSC2 mutations (Au et al.

Published online: 10 July 2013

2007; Dabora et al. 2001; Jansen et al. 2008). Neurodevelopmental manifestations are common and include severe epilepsy, cognitive impairment, attention deficit hyperactivity disorder, and autism spectrum disorder (ASD) (Harrison and Bolton 1997; Bolton et al. 2002; Jeste et al. 2008). The cognitive outcome of TSC varies significantly between patients, even among individuals with the same type of neuroanatomical abnormalities. Some patients have normal cognitive function, but as many as 40 % have learning disabilities, and more than 60–80 % suffer from epilepsy at some point in their life (Shepherd and Stephenson 1992; Holmes and Stafstrom 2007; Crino et al. 2006). A number of studies have also shown that up to 50 % of individuals with TSC may also develop ASD (Harrison and Bolton 1997; Guttierez et al. 1998; Muzykewicz et al. 2007), but the risk factors for ASD in these patients are not clearly understood (Numis et al. 2011).

While many studies have described the clinical characteristics of children with TSC and ASD, few studies have investigated the functional mechanisms that underline the association between the two disorders. There is increasing evidence that ASD is associated with aberrant connectivity between brain regions (Kleinhans et al. 2008; Nebel et al. 2012) and abnormal information processing and integration, e.g., McGrath et al. (2012). Based on limited imaging studies, there is also some evidence of loss of white matter structural integrity in children and young adults with TSC (Peters et al. 2012), and abnormal connectivity in parietal regions (D'Argenzio et al. 2009). However, the electrophysiological correlates of structural abnormalities in TSC remain elusive. There is one report of high gamma (>50 Hz) activity in the brain area surrounding cortical tubers (Irahara et al. 2012), and the presence of tubers has been correlated with increased epileptiform activity (Gallagher et al. 2009; Major et al. 2009; Jacobs et al. 2008). However, potential effects of structural abnormalities on fundamental aspects of neurodynamics, such as dominant brain rhythms and their spatio-temporal distributions, have not been investigated. It is of significant interest to identify potential neurodynamic abnormalities, including aberrant information processing and coordination between brain regions in TSC. Such abnormalities may help explain differences in the cognitive outcome of the disorder, its correlation with ASD, and facilitate early diagnosis and identification of patients with TSC who may be at high risk of developing ASD.

This study investigated dominant brain rhythms in infants with TSC, in the age range 18–30 months, using novel signal processing approaches for analysis of high-density scalp electroencephalograms (EEG). Specifically, using a data-driven approach [a modified empirical decomposition (Huang et al. 1998; Stamoulis and Betensky 2011)], characteristic EEG frequencies were estimated in the range 1–250 Hz. Until recently, EEG studies have assumed that scalp EEG does not contain useful information of neural origin at frequencies above 50 Hz, because of the assumption that the skull and scalp act as filters that attenuate higher frequencies. The ratio of the conductivity of the brain to that of the skull has been assumed to be typically $\sim$1:0.0125, at least in adults (Geddes and Baker 1967). However, more recent studies have proposed a more realistic ratio of $\sim$1:0.065, resulting in significantly less attenuation of signals propagating through the skull (Oostendorp et al. 2000). Infants and children have thinner skulls, which may also make it easier to measure higher frequencies. Finally, in theory the skull and scalp would not filter out activity up to at least $\sim$250 Hz. Instead, a more plausible explanation may be that high frequency activity reflects network correlations over shorter distances in the brain and/or activity from localized sources, i.e., with limited propagation, which may be more heavily filtered by the passive properties of the head. Using a novel denoising approach to suppress artifacts and eliminate noise-related components in the EEG, we estimated characteristic frequencies significantly higher than 50 Hz in non-task/resting and in visual task-related EEGs. Three groups of age-matched TSC and healthy infants were analyzed: 18, 20–24 and 28–30 months. We found EEG rhythms with significantly higher characteristic frequencies in TSC than in healthy infants, at ages $\geq$20 months. These frequencies were modulated by visual tasks, i.e., decreased during the presentation of object and face (mom versus stranger) images. Both resting/non-task and task-related characteristic EEG frequencies in the ripple and gamma range decreased significantly with increasing age in healthy infants, suggesting that neural maturation may be associated with a shift in the peaks of the EEG spectrum (corresponding to dominant frequencies), to a lower range. Their rate of change in infants with TSC was significantly slower. This study presents novel insights into electrophysiological mechanisms, such as abnormally high and spatially distributed high-frequency neural activity, that could destructively interfere with information processing in the brain, and consequently impair cognitive function in TSC.

Methods

Experimental Data

All EEG data were collected in the Laboratories of Cognitive Neuroscience, Boston Children's Hospital. Two datasets were analyzed in this study. The first included 10 infants with TSC, age 18–30 months ($\mu = 23.3$, $\sigma = 4.94$ months), 3 healthy infants age 18 months and 3 healthy infants at 24 months. The second dataset included 6 healthy infants, age 20–30 months ($\mu = 22.8$, $\sigma = 3.7$ months). Therefore,

data from a total of 10 infants with TSC and 12 controls were analyzed. Data from each subject were analyzed separately. TSC is often diagnosed perinatally, and thus all infants with TSC had a confirmed diagnosis of the disorder, and no other diagnoses that were not consistent with TSC. All control subjects were neurologically healthy, with no immediate family history (parents/siblings) of neurodevelopmental disorders. Additional inclusion criteria were enrollment in the study prior to one year of age, and normal or corrected to normal vision. Infants with a history of prematurity (<37 weeks gestational age) or birth trauma were excluded.

The first dataset was recorded using a 128-channel Hydrocel Geodesic Sensor Net (EGI, Inc., Eugene, OR, USA), and a sampling rate of 500 samples/s. Based on the Nyquist sampling criterion, this theoretically allowed the discrimination of frequency components up to 250 Hz. The second dataset was recorded during an earlier experiment, using a 64-channel Geodesic Sensor Net (also from EGI), and a sampling rate of 250 samples/s. Both electrode net densities cover the entire head surface and contain sponge-based carbon fiber electrodes (Ag/AgCl-coated, carbon-filled plastic electrodes with a sponge). Prior to fitting the sensor net over the scalp, the sponges were soaked in a solution of 6 ml KCl/L of distilled water and 5 ml of baby shampoo, to facilitate electrical contact between the scalp and the electrode. In the analysis, only data from electrodes that correspond to the 10-10 international equivalent system were used (EGI Technical Note 2005). Thus, a common set of 56 channels were included in the analysis of both datasets.

The experimental paradigm is summarized in the diagram in Fig. 1. EEG was collected as infants sat on their mother's lap. Resting data were first collected for ~2.5–6 min, to ensure that sufficiently long baseline signals were available for analysis. Typically, the researcher running the experiment would blow bubbles during this time interval, to ensure the infant's compliance with the quiet and darkened room while wearing the sensor net. This was followed by a block of ~50 visually-evoked potential (VEP) trials (~500 ms in duration), during which alternating images of a checkerboard and its contrast were presented on the screen. Following the VEP paradigm, subjects were shown images of familiar and unfamiliar faces, i.e., mom and strangers, and unfamiliar objects (toys). Each picture remained on the screen for ~500 ms, followed by an inter-stimulus interval that was based on the infant's attention to the screen, and was on average ~1–4 s. The inter-stimulus interval varied widely as the experimenter only presented the next stimulus when the infant was attending to the monitor, as their behavior was monitored via a video camera mounted above the presentation screen. In some cases this interval was as long as 10 s. EEGs were continuously recorded during the paradigms. The dataset from the 64-channel system included EEGs recorded during the presentation of familiar-unfamiliar faces, and non-task EEGs during the inter-stimulus intervals, i.e., there was no resting EEG available. Also, no other experiments were performed during the collection of these data. EEG recorded prior to any task is hereafter referred to as *resting*, while signals recorded during inter-stimulus intervals are referred to as *non-task*.

Signal Processing Methods

EEG Preprocessing

Continuous EEG signals were analyzed using Matlab (Mathworks, Inc, Natick, MA, USA). Signals were first highpass filtered with a cutoff at 0.3 Hz, using NetStation waveform tools. EGI systems set a low-pass anti-aliasing filter with a cutoff either at the Nyquist frequency or higher. All data were first filtered with a stopband filterbank of third-order elliptical filters centered at the 60 Hz harmonics of powerline noise, i.e., at 60, 120, 180, 240 Hz for data sampled at 500 samples/s and at 60, 120 Hz for data sampled at 250 samples/s. The filter parameters were 1 Hz bandwidth, 20 dB attenuation in the stopband and 0.5 dB ripple in the passband. EEG signals were filtered in both forward and reverse directions to eliminate potential phase distortions due to the non-linear phase of the filter. Eye blink artifacts, which often contaminate scalp EEGs, were suppressed using a stopband matched-filterbank (Stamoulis and Chang 2009). For each subject, the eye-blink waveform was estimated from its multiple occurrences in the recordings, to construct the template of the matched-filter, which in this case was used as a stopband filter. Signals were matched-filtered in both forward and backward directions to eliminate potential phase shifts. EEGs from infants with TSC are likely to include interical spikes. We carefully examined these signals for spike occurrence. There were only few EEG segments (trials), predominantly task-related, that included spikes in a subset of the electrodes. These trials (all channels) were removed from the analysis.

Estimation of Characteristic EEG Frequencies

Estimation of dominant frequencies from the peaks of the EEG spectrogram is often a difficult process. It requires segmentation of the data to compute their Short-Time Fourier Transform (STFT) in order to account for the spectral non-stationarity of the EEG. It is often difficult to identify dominant peaks in EEG spectra, particularly at high frequencies. An example of 3 EEG spectra, estimated from the same channel (C1) in consecutive 5-s segments is shown in Fig. 2. For each segment, the spectrum was estimated both using a conventional Fast Fourier Transform (FFT)

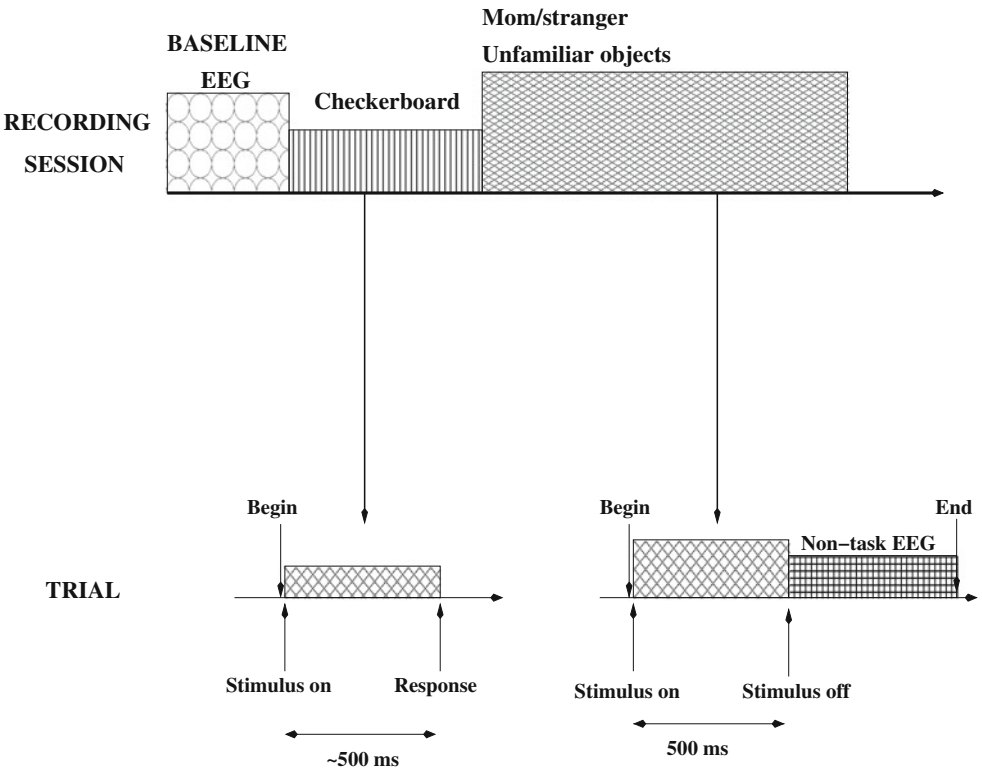

Fig. 1 Diagram of experimental paradigm and recording session (*top*), and intervals of checkerboard and mom/stranger and unfamiliar objects (*bottom*)

(top plots) and Thompson's multi-taper spectrum (Thomson 1982) (bottom plots), to account for the spectral leakage and thus bias in the FFT spectral estimate. In both sets of plots, in addition to differences in the frequency of dominant peaks, it is difficult to robustly and consistently identify these peaks. Therefore, the majority of EEG studies examine signal energy in biologically relevant bands (typically δ to γ). Although the energy of the EEG in healthy brains may fall well within these bands, modulations of cortical rhythms by anatomical abnormalities are poorly understood. Furthermore, different regions of the brain may have somewhat distinct dominant frequencies within these bands, which may be difficult to estimate from spectra. Alternative methods are, therefore, necessary.

Signal Decomposition Using a Modified Empirical Mode Decomposition (EMD) There are very few methods for time-frequency analysis and decomposition of non-stationary signals that make no a priori assumptions on the shape of the unknown signal components (hereafter referred to as modes). Widely used wavelet-based methods make an initial assumption on the mother wavelet, and are thus not entirely data-driven. The most-widely used alternative method is the *Empirical Mode Decomposition* (EMD) (Huang et al. 1998), which recursively decomposes a non-stationary signal into components with significant amplitude contributions, each with a characteristic frequency. Therefore, each mode is a signal with a significantly smaller bandwidth than that of an entire biological band. A few previous studies have used this approach to analyze electrophysiological signals, e.g.,Burgess (2012), Tsai et al. (2012), Sweeney-Reed and Nasuto (2009).

The EMD approach involves fitting upper and lower envelopes through local extrema of the signal, computing the mean of the two envelopes and subtracting this mean from the original signal. This sifting process is typically repeated several times, at each iteration subtracting a new mean from the signal obtained in the previous iteration, until the standard deviation (SD) computed from signals at two consecutive iterations reaches a stopping threshold (typically 0.1–0.3; here we used a SD threshold of 0.1). The resulting signal from this process is an *intrinsic mode function* (or mode). Once a mode is estimated, it is subtracted from the original signal and the sifting process is repeated with the residual signal, to obtain the next mode. The entire estimation stops once the mean square error (MSE) between the original signal and the mode-based re-synthesized signal, i.e., the linear superposition of n estimated modes, is small. No upper bound is set on the number of modes, but n is typically small ($\leq$20), at least in electrophysiological signals in the frequency range of interest. Decomposed modes satisfy two conditions: (1) they have zero mean and (2) they contain a single extremum between zero-crossings. However, the original EMD method may not discriminate biologically relevant signal contributions from high-amplitude noise contributions. Modifications have been proposed, to eliminate modes

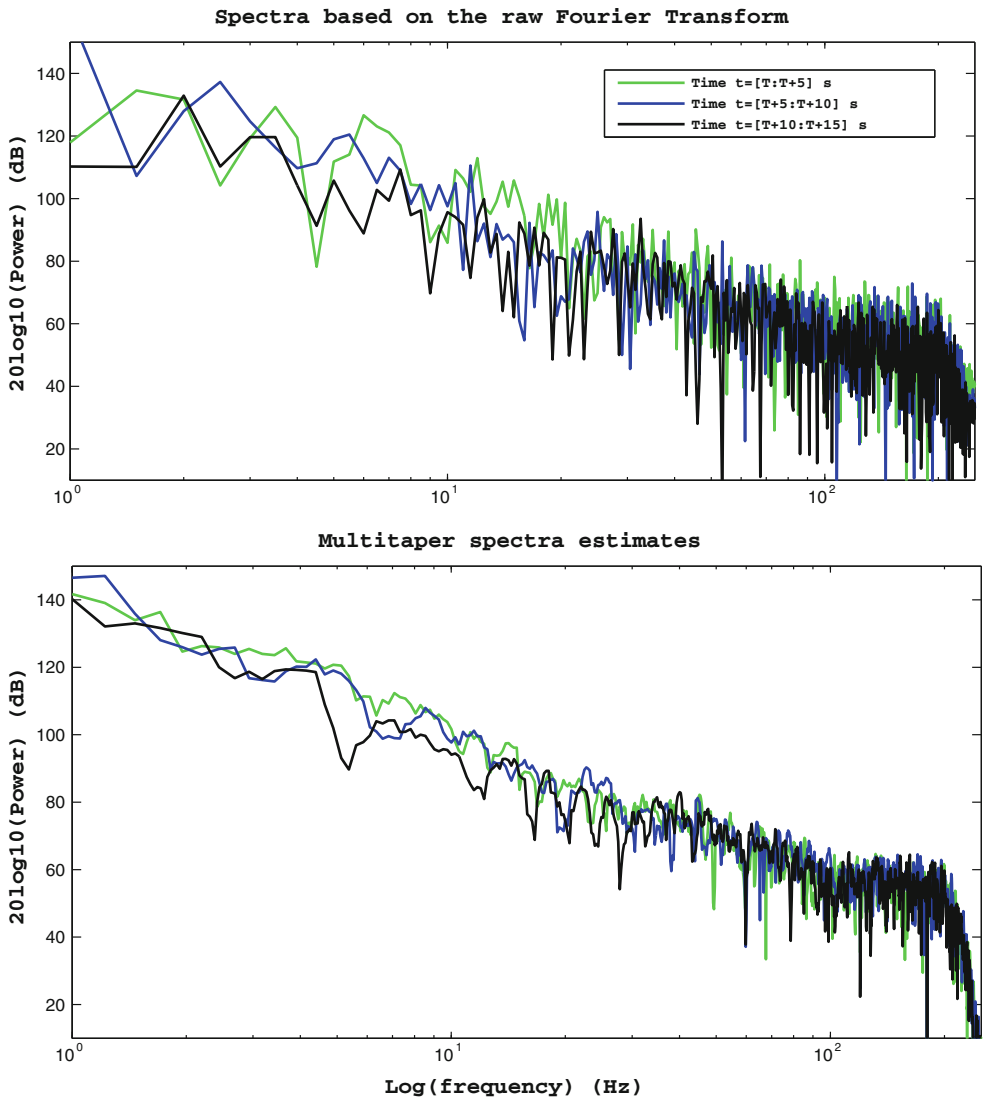

Fig. 2 Example of channel C1 EEG spectra, estimated at 3 consecutive 5-s segments from resting signals, using the Fast Fourier Transform (*top plots*) and Thompson's multi-taper spectrum, using a time-bandwidth product = 3.5 (*bottom plots*). *Each color* corresponds to a different time interval. The data are from baseline signals from one healthy infant at 18 months (Color figure online)

potentially associated with noise, while maintaining the overall structure of the signal. In fact, EMD may be used for denoising purposes to remove noise contributions and artifacts (Stamoulis and Betensky 2011; Sweeney et al. 2012). Here, each EEG signal was mode-decomposed using EMD, and the risk function proposed in Stamoulis and Betensky (2011) was then used to sequentially eliminate noise-related components. The auto-correlation of remaining components was then calculated, both to estimate the characteristic frequency of each component, but also to determine whether this component may still represent a noise contribution to the signal that was not previously eliminated. An example of a baseline signal segment from one EEG channel and a subset of its modes (8 of 14 estimated modes) are shown in Fig. 3. A simulation showing signal synthesis using a time-varying weighted superposition of sine waves with distinct frequencies, contamination by additive Gaussian noise and decomposition using the EMD procedure is shown in Fig. 4. The difference between modal frequencies estimated from components obtained through EMD and original modal frequencies varied between 0.5 and 3 Hz, from low to high frequencies. This simulation demonstrates that the EMD method correctly estimates the underlying structure of a non-random signal, and may be used to eliminate noise-related components. Note that EMD has also been used to study the characteristics of random signals, showing that a random signal may be decomposed into components with structure, when the original signal is white noise (Wu and Huang 2004).

Auto-Correlation and Zero-Crossing Methods for Frequency Estimation Both autocorrelation analysis and simple counting of the number of points at which a modal signal crosses the x-axis (zero-crossings) have been widely used to estimate the characteristic frequency of signal modes (Markel 1972; Phadke et al. 1983). The zero-crossing method is more sensitive to the noise level of a signal than the auto-correlation method. Here, all signals were denoised and individual modes with high signal-to-noise ratios (SNR) were extracted. Both methods were used to obtain estimates of modal frequencies. The differences between estimates were consistently non-significant ($\leq$2 Hz for frequencies 20–150 and $\leq$0.6 Hz for lower frequencies). Furthermore, the auto-correlation function was used to assess whether a modal signal was random. Although this process may not ensure that the original signal from which the mode was estimated is not just noise, it does assess whether the estimated mode is non-random based on its autocorrelation. An example of autocorrelation functions for the 3 highest-frequency modes, estimated from one healthy infant and one infant with TSC, both at 18 months (a 2-s signal from channel P9) is shown in Fig. 5. Each panel corresponds to one mode. The characteristic frequencies for the first and second modes were substantially higher in TSC (142.8 and 77 Hz, respectively). The autocorrelation function for a white noise signal is superimposed to the autocorrelation functions of the modes.

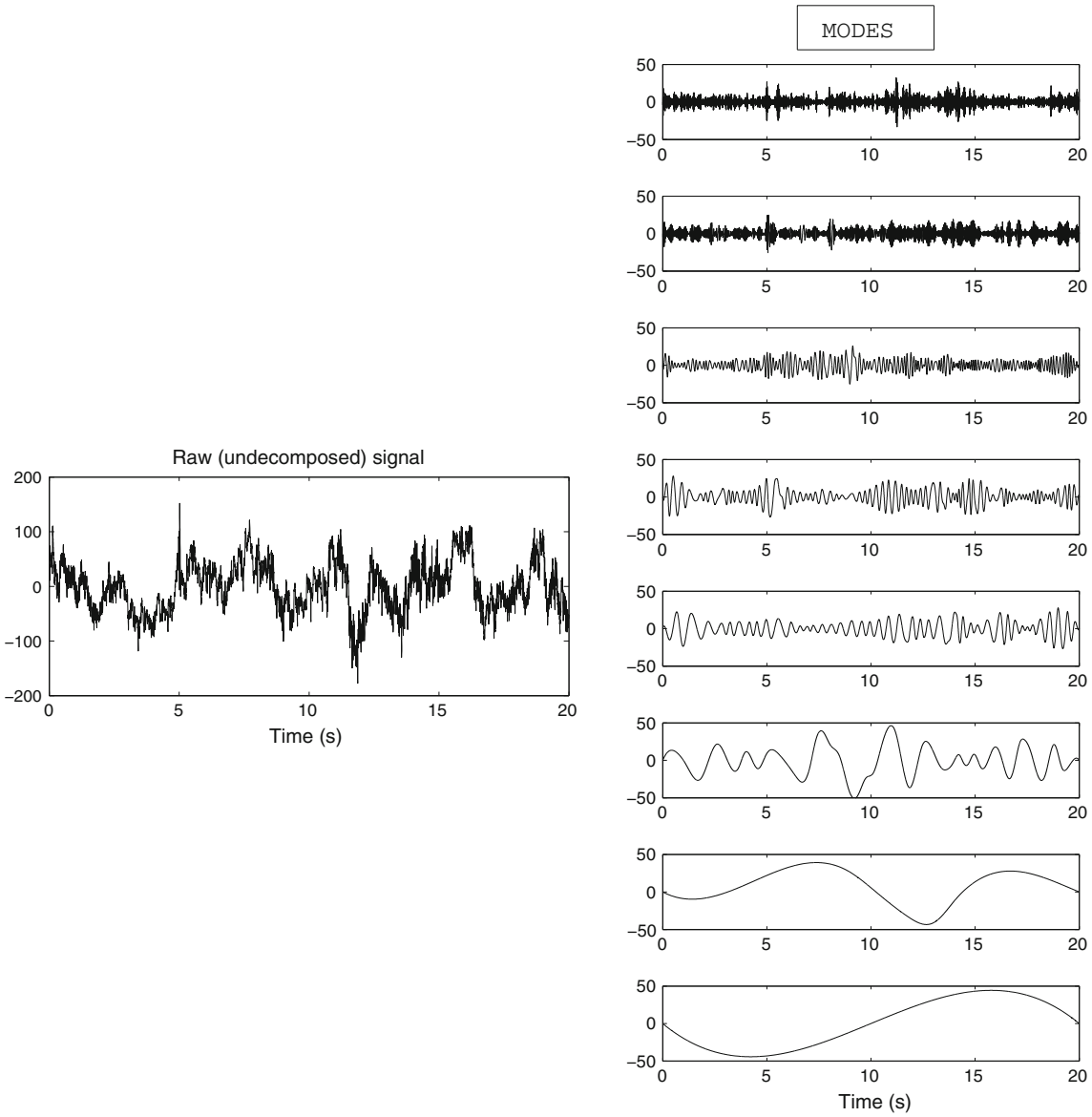

Fig. 3 Raw EEG segment from one channel (*left plot*), and a subset of decomposed modes (*right panels*), including very low-frequency modes (<5 Hz, *bottom plots*) and higher frequency modes ($\geq$40 Hz, *top plots*)

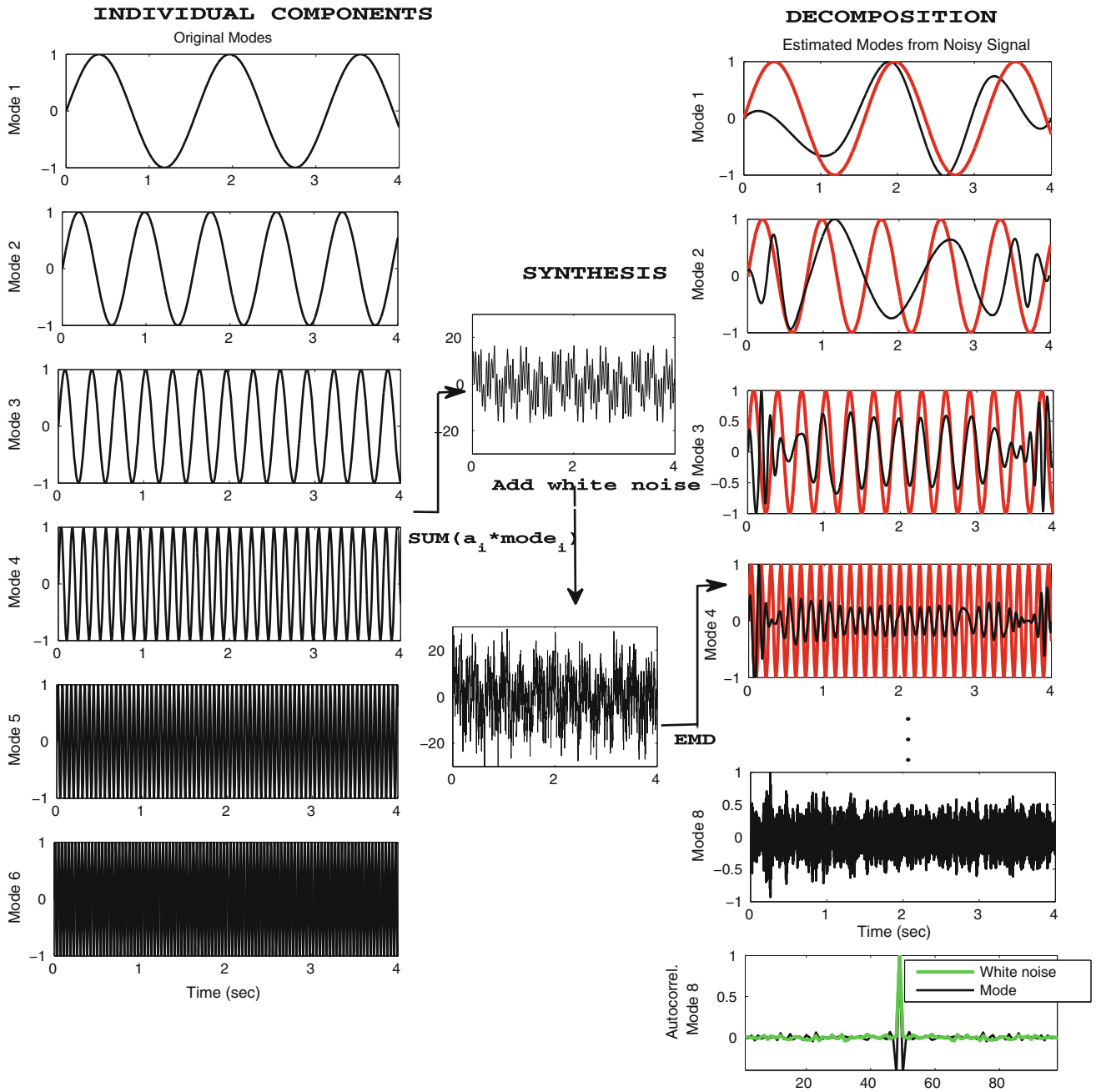

Fig. 4 Simulation of 6 modes (*sine waves*), with characteristic frequencies up to 45 Hz (*left column*). A time varying (at two time intervals 0–2 and 2–4 s) superposition of these modes was used to synthesize a non-stationary signal, which was then contaminated with additive Gaussian noise. Using the proposed EMD approach, the resulting signal (*middle column*) was decomposed into 10 modes, 6 modes with approximately the same frequencies as the original modes (errors in estimated frequencies were in the range 0.5–3 Hz) 2 modes that were noise-related, based on their autocorrelation functions, and two very low-frequency (<0.5 Hz) that are not typically included in the analysis, i.e., we did not examine modes with characteristic frequencies less than ~1 Hz. The autocorrelation of one of the quasi-random components is shown in the *right column*, *bottom panel*. Note that estimated modes had different amplitudes, based on their respective contributions to the signal. However, they were normalized to ±1 for plotting purposes, to compare their shapes to the original modes

The original (raw) EEG signals from which modes are estimated are non-random, but are a superposition of neural oscillations and noise. By definition, the EMD process estimates high-frequency modes first, since it fits envelopes through local minima and maxima, i.e., first through the many local minima and maxima associated with higher frequency contributions. The number of these extrema decreases as more modes are estimated and subtracted from

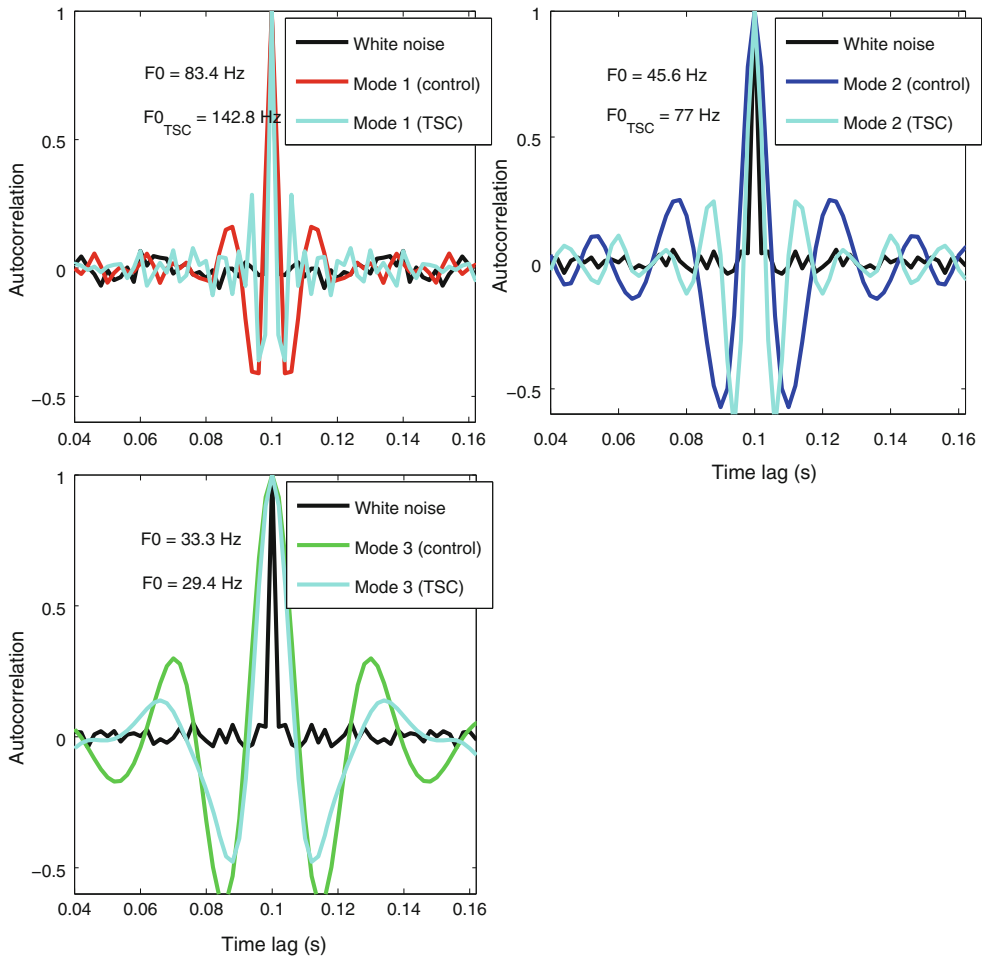

Fig. 5 Autocorrelation functions for modes above and within the gamma-band range. The highest-frequency mode autocorrelation is shown in *top left panel*, and the two gamma modes in the *top right* and *bottom left panels*. The autocorrelation of a white noise signal is superimposed (*black curves*). In *each panel*, respective modes from the EEG of a TSC subject (*cyan curves*) are superimposed to modes from the EEG of an age-matched healthy control (*red*, *blue*, *green curves*). The estimated characteristic frequencies are also noted (Color figure online)

the original signal, and ultimately the lowest-frequency mode is estimated. Thus, the raw EEG signal based on which the EMD estimation starts with is non-random. Although it is possible to estimate oscillatory components from white noise signals using EMD, and in fact this approach has been used to investigate the characteristics of white noise (Wu and Huang 2004), in such a case the original signal is pure noise but the modes may be artifactually oscillatory. Here, the highest frequency and subsequent components were estimated from a non-random raw EEG signal, and through examination of their autocorrelation functions only non-noise contributions to the original signal were further analyzed. It is possible that if the noise level in the raw signal is high, the extrema through which the first set of upper and lower envelopes are fitted may correspond to noise peaks, but this will be reflected in the first mode and its autocorrelation, i.e, the mode will represent a noise contribution to the original signal.

Statistical Analysis The small sample size in each subgroup (3–4 subjects) precluded the development of regression models for comparing trial, space- and/or time-averaged modal frequencies between age subgroups, i.e., there was no sufficient statistical power for such analysis. With 3–4 data points per sample, the results even from simple non-parametric statistical comparisons may not be truly meaningful. However, when spatial modal frequency patterns were averaged over subjects in an subgroup, resulting in samples with 56 data points each (corresponding to the number of EEG electrodes), the non-parametric Wilcoxon rank-sum test was used to compare these patterns between subgroups. Admittedly, these tests are non-optimal, since dominant frequencies may be clustered-correlated in space (in different regions of the brain), but the small sample limited the extent of the statistical analysis. For each recording condition, individual dominant modes in the 18-month subgroup was compared to the 20–24-month subgroup, and the latter to the 28–30 month

subgroup to detect age-related effects. The goal of these comparisons was to assess potential TSC-related effects on individual modal frequencies, at individual ages, separately for different recording conditions (resting, task-related, non-task).

Results

We compared the spatio-temporal distribution of dominant EEG frequencies in TSC and healthy infants at 18, 20–24 and 28–30 months, grouped according to the age clustering of the TSC cohort, i.e., there was no age continuity in the sample, only 3 clusters at the above ages. In addition to resting and non-task EEG, recordings from VEP, familiar/unfamiliar faces and unfamiliar object trials were also separately analyzed. Only a subset of subjects (3 controls at 18 months, 1 control at 24 months and all 10 infants with TSC) had recordings during all tasks. All subjects had non-task data (from inter-stimulus intervals), and data from trials of familiar/unfamiliar faces. Mode decomposition was applied separately to each signal. Although there was no a priori selected upper bound on the number of estimated of modes, typically a small number of modes was estimated ($\sim$9–10 modes).

Baseline and Non-task Fundamental Frequencies

We first examined the spatio-temporal distribution of resting and non-task dominant EEG frequencies in healthy and TSC infants. 'True' baseline signals, i.e., prior to any task, were available only for 3 controls, all age 18 months and all infants with TSC.

Temporal Variability of Characteristic Frequencies Resting EEGs were typically much longer than a few seconds. Thus, they were first segmented into 2-s windows, and modes and their characteristic frequencies were estimated in each window. This allowed us to assess the variation of these frequencies over time. To compare between subgroups, dominant frequencies in the same range were averaged over all electrodes, to create one temporal profile per frequency for each subject. As EEG recordings varied in length between subjects, these profiles were aligned at $t = 0$, and then averaged over subjects in the same subgroup. The duration of the resulting temporal profile was the common duration between subject-specific profiles. Figure 6 shows the temporal (averaged over all electrodes) variation of 5 baseline modal frequencies in the range 10–200 Hz. Resting EEGs from healthy subjects were slightly shorter. Modal frequencies >60 Hz were higher in TSC than in controls consistently across time. Dynamic fluctuations of modal amplitudes were substantially higher in TSC, but lower-frequency modes (lower gamma, beta and alpha) had higher amplitudes than ripples and high-gamma modes.

Spatial Variability of Characteristic Frequencies Figures 7 and 8 show the spatial (time-averaged) variability of baseline characteristic frequencies. Individual frequencies, estimated using in 2-s sliding window from each EEG, were averaged in time (at each electrode), and across subjects within a particular subgroup. Thus, for each age subgroup (TSC or control) a spatial map of the distribution of frequencies in the brain was estimated. The highest modal frequency was observed in centro-parietal and parietal regions, and was significantly higher and more uniformly distributed in space in TSC than in healthy infants ($p < 0.0001$, CI [3.32, 6.21] Hz). This was also the case for the high-gamma mode, estimated in the frequency range 65–82 Hz. This mode was, however, more spatially localized in centro-parietal/parietal channels ($p = 0.003$, CI [0.72, 3.45] Hz). There were no statistically significant differences in lower gamma ($p = 0.28$) and beta ($p = 0.33$) frequencies between TSC and healthy infants. There were no overall statistically significant differences in alpha and theta modal frequencies between TSC and controls, but both frequencies were more uniformly distributed in space in healthy infants, and more localized in temporal and fronto-temporal regions in TSC. Therefore, characteristic frequencies of fronto-central and central areas in the alpha and theta range were higher ($\sim$10 %) in healthy infants, whereas corresponding frequencies in temporal and fronto-temporal regions were higher ($\sim$10–15 %) in TSC. Finally, there were no statistically significant differences in delta frequencies between groups.

Given the data availability, in order to examine the variation of modal frequencies and their amplitude across all age groups, we estimated these parameters from non-task EEGs, in the intervals following completion of image trials (see Fig. 1). The highest modal frequency estimated from non-task EEG signals in TSC subjects was $\sim$162 Hz. Similarly to baseline (resting) signals, high-frequency modes had low amplitudes and were spatially distributed in large areas of the brain. They were primarily detectable in 18–24 month old infants with TSC. Corresponding modes in healthy subjects had significantly lower frequencies. The highest modal frequency estimated in healthy infants was 147 Hz at 18 months and 138 at 24 months, the latter only in very few electrodes. On average, the highest frequencies were $\leq$90 Hz at 24 months, and thus at least 40 Hz lower than the average ripple frequencies at 18 months. In EEGs from controls recorded in the same age range (20–24 months) but with a sample rate of 250 samples/s, the highest estimated frequencies were $\leq$80 Hz. The differences between 20–24 month subgroups sampled at different sampling rates was of the order of inter-subject variability of these frequencies within each subgroup. This suggests that

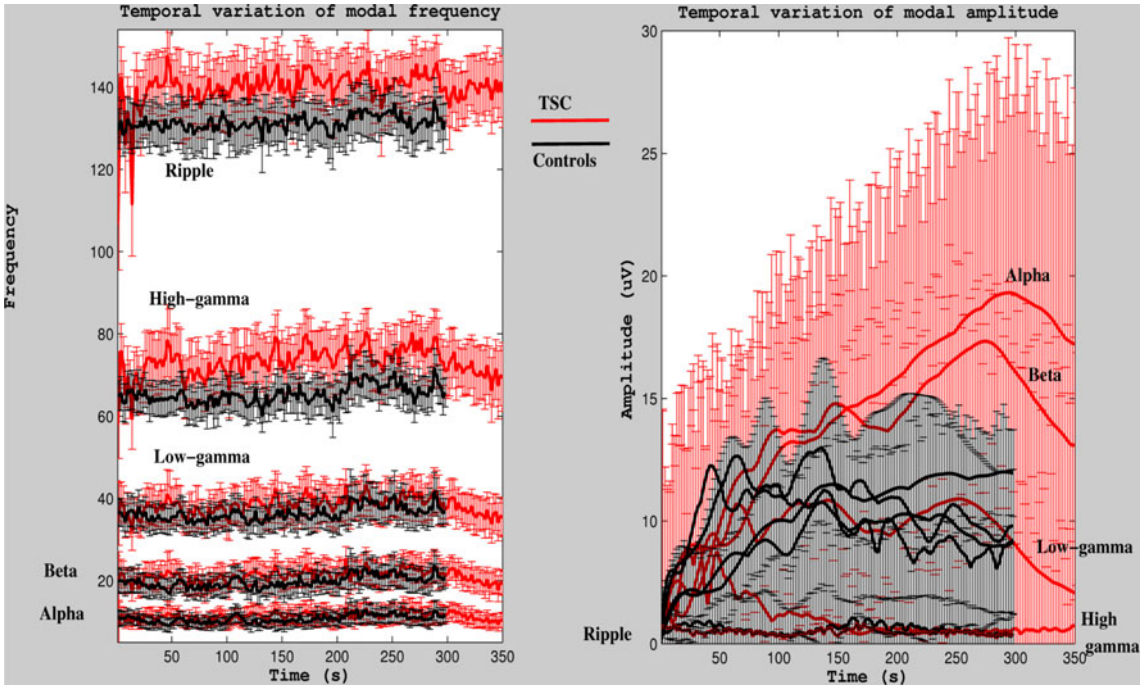

Fig. 6 Temporal variation of baseline modal frequency (*left*) and amplitude (*right*) in TSC (*red curves*) and healthy (*black curves*) subjects. Only the first 5 modes are shown (in the frequency range 10–200 Hz). Data were averaged over channels, and subjects in the 18-month subgroup, for which baseline was available. The inter-subject and inter-channel variability at superimposed (±1 SD) (Color figure online)

estimated differences between age ranges may be unrelated to differences in sampling rate. Similarly, the highest estimated frequency in healthy infants at 28–30 months was also ≤80 Hz. Thus, EEGs from healthy subjects 20–30 months did not have the highest (ripple) mode, only gamma modes with frequencies <90 Hz. The spatial distributions of the two highest modal frequencies (in the ripple and high-gamma range) in non-task EEGs are shown in Figs. 9, and 10 for the subset of healthy subjects with data at 18 and 24 months, sampled at 500 samples/s. Only the two highest frequencies were statistically distinct in TSC ($p < 0.01$). Signals were averaged over trials and subjects within each age subgroup (3 in each subgroup, except the 28–30 TSC sub-group which included 4 subjects). These results indicate that the dominant spectral peaks of the EEG at >50 Hz occur at higher frequencies in infants with TSC than in healthy controls at ages ≥20 months.

In summary, measurable signal power was detected at frequencies >100 Hz in non-task EEGs at 18 months, both in infants with TSC and in controls. Dominant modal frequencies in TSC were, however, at least 10 % higher. These frequencies decreased with age, at distinct rates in the two cohorts. Specifically, estimated high frequencies in TSC at 20–24 months and 28–30 months were at least 20–30 Hz lower than at 18 months, i.e., the spectral content of the EEG shifted towards lower frequencies with age. In healthy infants, a more substantial decrease in high modal frequencies occurred earlier, i.e., by 20–24 months, the ripple frequency was no longer detectable in the EEG. Overall, the highest modal frequency in controls at 20–24 and 28–30 months were ≤90 Hz.

Familiar/Unfamiliar Face Trials

We compared modal frequencies in EEGs recorded during the presentation of mom and stranger images, respectively. The highest estimated frequency during these trials was substantially lower than the corresponding frequency in non-task EEGs, in all groups, and across channels. The results are summarized in Fig. 11 for the ripple and gamma (high and low) modes, respectively, as a function of age. Data were averaged over trials, channels and subjects within each subgroup. At 20–24 months, both data sampled at 250 samples/s (blue) and data sampled at 500 samples/s (black) are shown. The inter-subject variability (±1 SD) are superimposed to the mean modal frequency. Frequencies estimated from trials during presentation of images of mom were overall identical to those estimated during presentation of stranger pictures, i.e., there were no condition effects. Statistically significant differences were estimated between the highest frequency modes in TSC and healthy infants at ages 20–30 months (>30 Hz difference in both mom and stranger trials). Given that modal frequencies vary significantly between brain regions, it was more meaningful to statistically compare frequency vectors across channels (not shown here), averaged over subject,

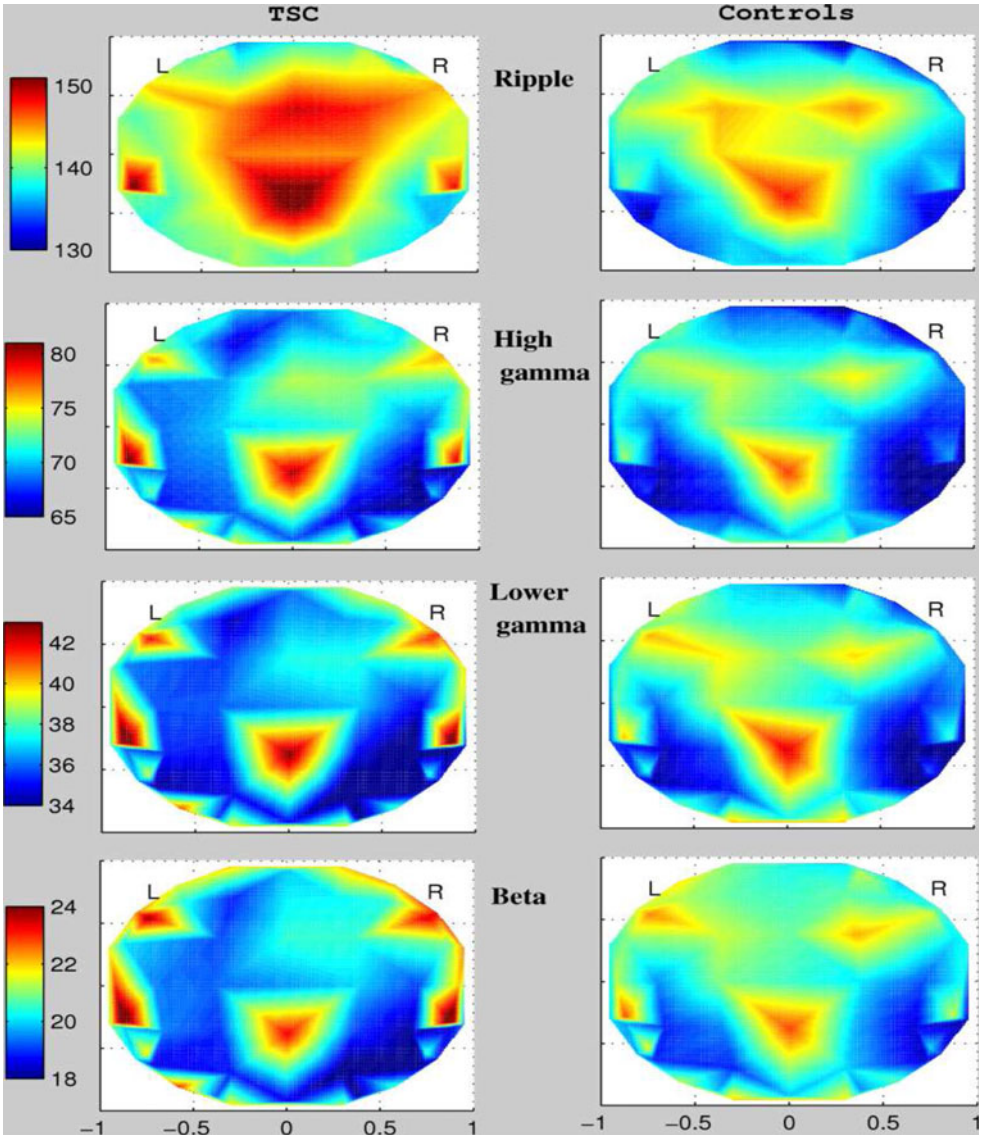

Fig. 7 Spatial distribution of estimated modal frequencies in the range >80, as well as lower- and higher-gamma beta bands, averaged over time and subject, in TSC (*left panels*) and health (*right panels*) 18-month infants. *Colorbars* represent frequency in Hz (Color figure online)

instead of grand averages over trial, subject and channel. Thus, whereas differences in ripple frequency between TSC and healthy infants were non-significant at 18 months ($p = 0.4834$), they were statistically significant at older ages: $p < 0.0001$, CI [20.6, 22.7] at 20–24 months, and $p < 0.0001$, CI [17.05, 21.8] at 28–30 months, in both mom and stranger trials. In older healthy infants, no modes in the ripple range were estimated. There were no statistical difference in modal amplitude between groups at each age.

We finally examined group differences in lower-frequency modes, shown in Fig. 12. There were no significant differences between TSC and control subgroups and/or mom/stranger trials at 18 and 24 months, in any modal frequency in the range 4–35 Hz, for all data sampled at 500 samples/s. There were statistically significant differences between TSC and controls at 20–22 and 28–30 Hz, but the control data were sampled at 250 samples/s. In theory, the sampling rate limitation should not affect estimated frequencies at ranges $\leq$30 Hz. Thus, the differences between healthy controls at 24 months and 20–22 months may be due to the small sample size, i.e., two randomly selected small groups.

In summary, we examined task-related modulations of the spectral content of the EEG across groups and ages. There was an overall shift towards lower frequencies from resting to familiar/unfamiliar face trial conditions across ages and groups. There was a statistically significant decrease in modal frequencies in the ripple and gamma ranges, between TSC and healthy infants at ages $\geq$20 months. No condition effects were found between mom and stranger trials. No consistent statistically significant differences were found at lower frequencies ($\leq$30 Hz) between TSC and controls.

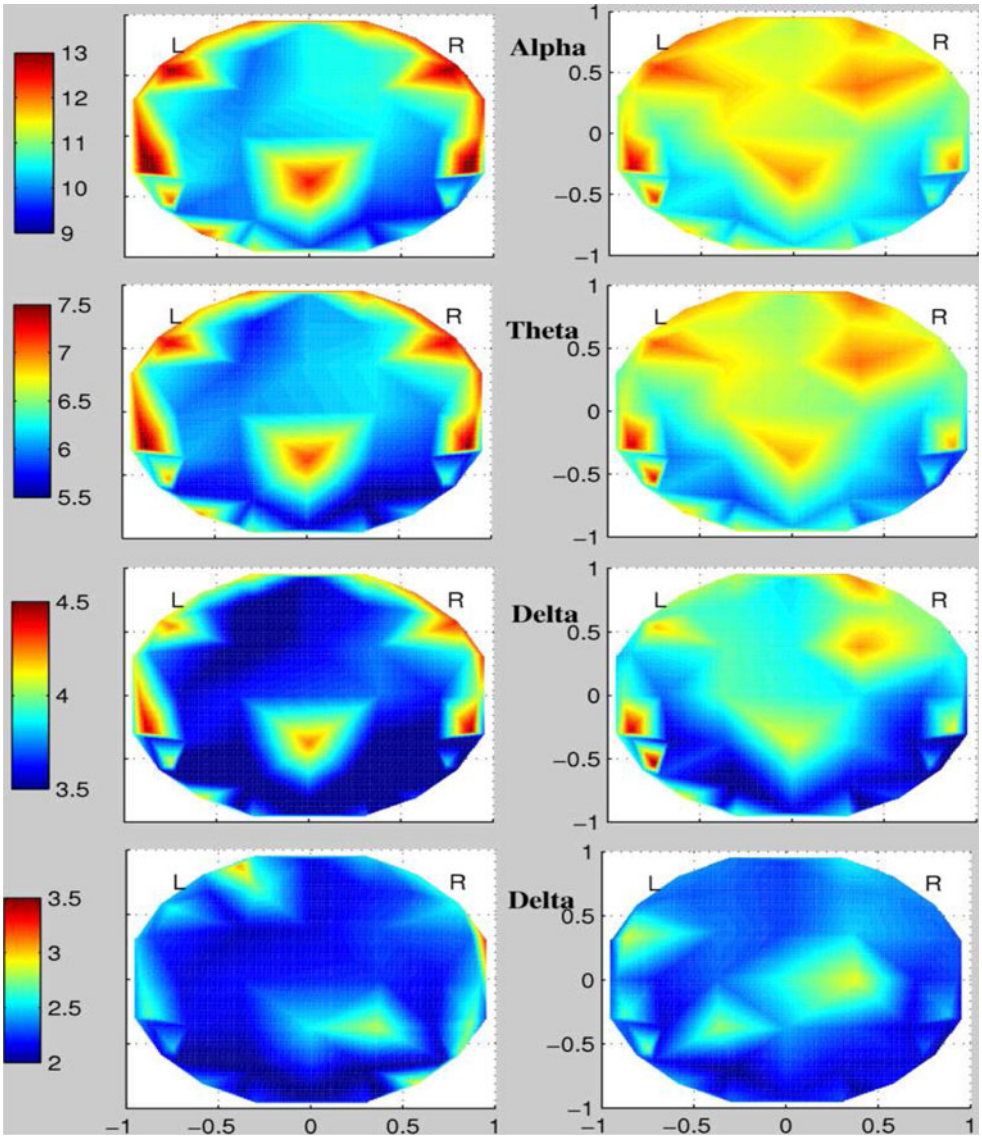

Fig. 8 Spatial distribution of estimated modal frequencies in the alpha, theta and delta bands (2 modes), averaged over time and subject, in TSC (*left panels*) and healthy (*right panels*) 18-month infants. *Colorbars* represent frequency in Hz (Color figure online)

VEP and Unfamiliar Object Trials

Finally, we examined the distribution of modal frequencies during the presentation of alternating checkerboards across TSC groups and in controls at 18 months, and during the presentation of unfamiliar object images. These paradigms were not used in the earlier experiment. For each subject, estimated frequencies were averaged over approximately 50 checkerboard trials, and separately over a variable number of object trials (typically about 20). For object trials, modal frequencies, their spatial, temporal and amplitude distribution varied in statistically identical patterns to those during the mom/stranger trials. During checkerboard trials, modal frequencies and their spatio-temporal distributions were identical to those during baseline and non-task trials. The spatial distribution of the ripple and two gamma-modes in the 3 TSC groups and the 18-month control group is shown in Fig. 13.

Discussion

We have estimated the dominant frequencies of scalp EEG in infants with TSC and age-matched controls, in the age range 18–30 months, using a data-driven signal decomposition approach based on EMD. We hypothesized that dominant EEG frequencies reflect cortical rhythms encoded in these signals, with measurable energy at frequencies above 80 Hz. High-frequency, non-noise related EEG contributions may represent a fundamental property of the developing brain, and may be affected by TSC. We have estimated these frequencies in baseline, non-task related

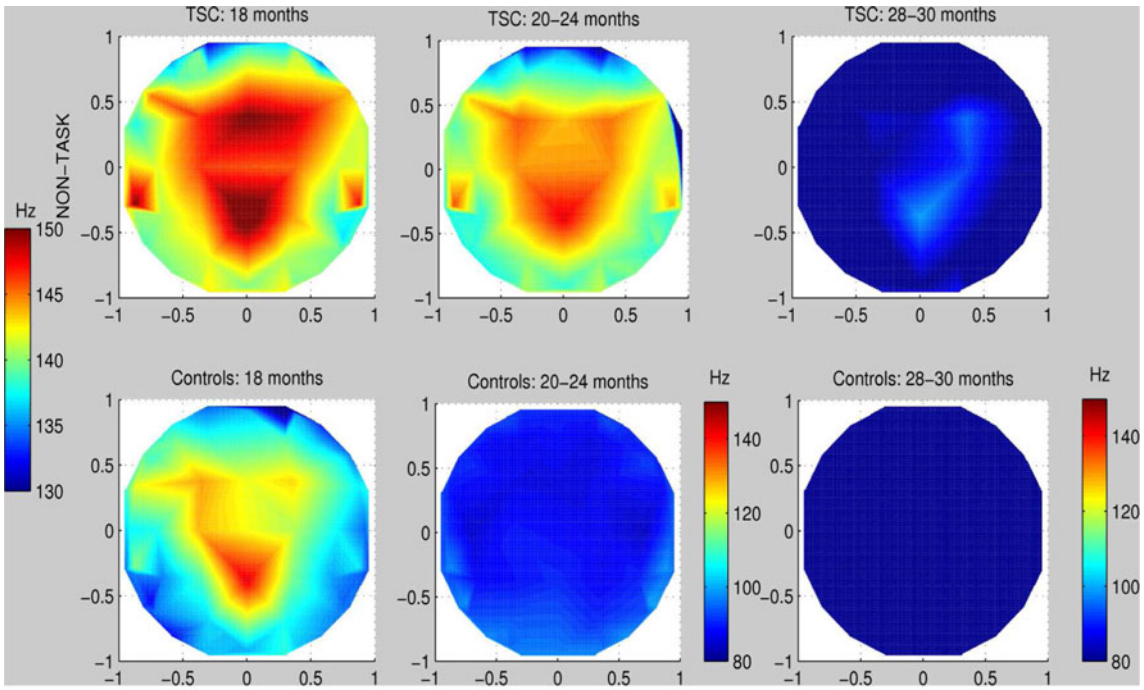

(a)

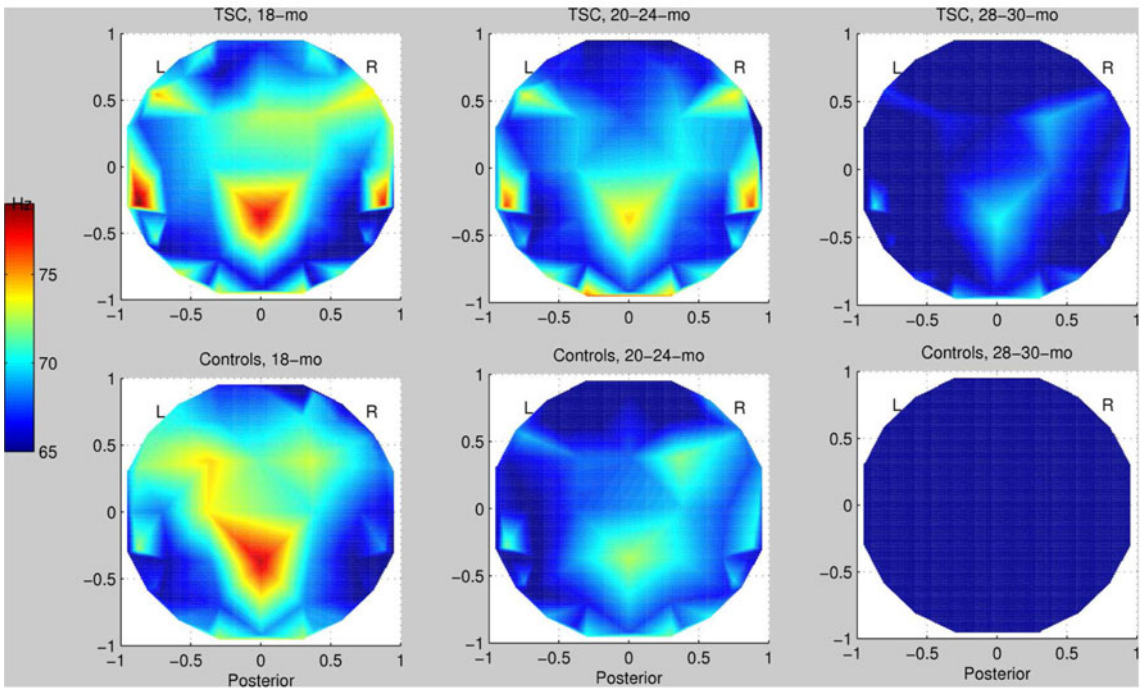

(b)

Fig. 9 Two highest frequency modes in non-task EEGs, estimated from multiple trials following presentation of mom/stranger images. Data were averaged over >40 trials and 3 subjects in the 18- and 20–24 month subgroups, and 4 subjects in the 28–30 TSC subgroup. *Left panels* correspond to the 18-month subgroup, middle panels to the 20–24 month subgroup and right panels to the 28–30 month subgroup. Data from all TSC subjects and 18-month controls were sampled at 500 Hz, and all data from 20 to 30 month controls were sampled at 250 Hz. *Colorbars* correspond to frequency in Hz; separate *colorbars* are shown for the older controls with significantly lower frequencies. **a** Spatial distribution of highest EEG modal frequency in TSC (*top panels*) and healthy infants (*bottom panels*) age 18–30 months. **b** Spatial distribution high-gamma modal frequency in TSC (*top panels*) and healthy infants (*bottom panels*) age 18–30 months (Color figure online)

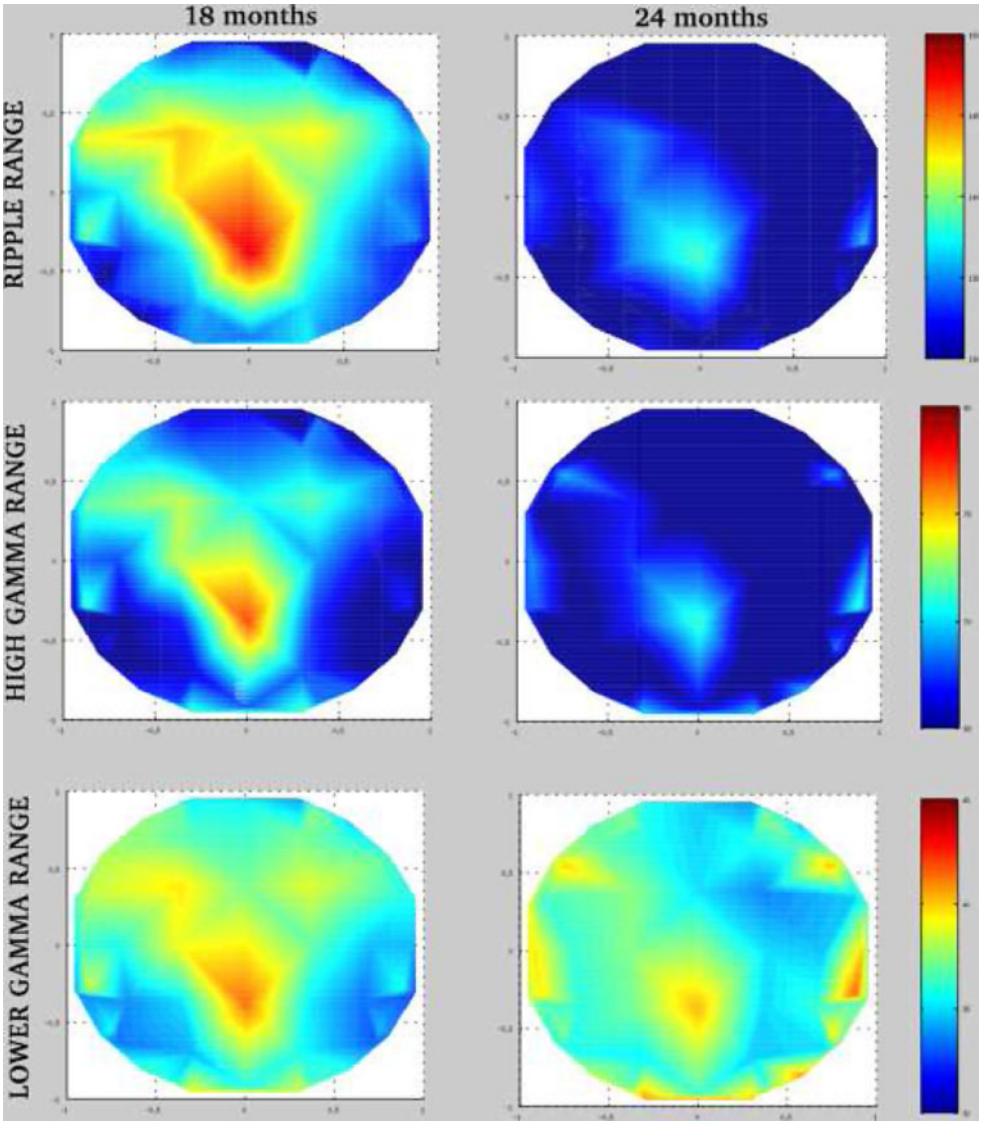

Fig. 10 Spatial distribution of estimated modal frequencies in the ripple (*top plots*) and gamma (high in *middle plots* and low in *bottom plots*), in healthy controls at 18 months (*left*) and 24 months (*right*), for non-task EEGs sampled at 500 samples/s. Colorbars correspond to frequency in Hz (Color figure online)

and visual task-related EEGs (during presentation of checkerboards, mom/stranger images, and unfamiliar object images). Each EEG signal was separately analyzed, parameter estimates were averaged either in space or time and across trials and subjects within the same age subgroup. Consistently higher modal frequencies were estimated in TSC subgroups than in controls.

First, a non-noise (based on its autocorrelation), low-amplitude but high-frequency (>80 Hz) mode was estimated in resting/non-task EEGs of 18–24 month-old infants with TSC and in controls at 18 months. This mode was broadly distributed in space, and thus present in a large number of EEG channels. Its highest frequency was observed in centro-parietal and parietal regions in both TSC and healthy infants. However, in healthy subjects it was substantially lower (on average 15–20 Hz lower). The amplitude of this mode was low (3–5 times less than other modes) and varied insignificantly between groups. Similarly, modes in the high-gamma (50–80 Hz) and lower-gamma (30–50 Hz) range, were also consistently estimated in all subjects. Again, corresponding modes in healthy controls had lower characteristic frequencies, particularly at 28–30 months, where the difference in frequency between TSC and controls was greater than 20 Hz. Given the low-amplitude and broad spatial spread of this activity in younger infants, high-frequency modes may correspond to noisy interference signals, possibly associated with redundant and/or developing neural circuits. High-frequency activity consistently decreased with age, possibly due to strengthening of functional connections and increased efficiency of neural transmission. In infants with TSC, the largest spectral shift, from ripple frequencies towards lower (gamma) frequencies occurred between 24–28 months. In contrast, in healthy infants this shift occurred earlier, between 18–20 months. Thus, by 20 months, low-amplitude high-frequency activity had significantly decreased in healthy subjects. Admittedly these observations are based on

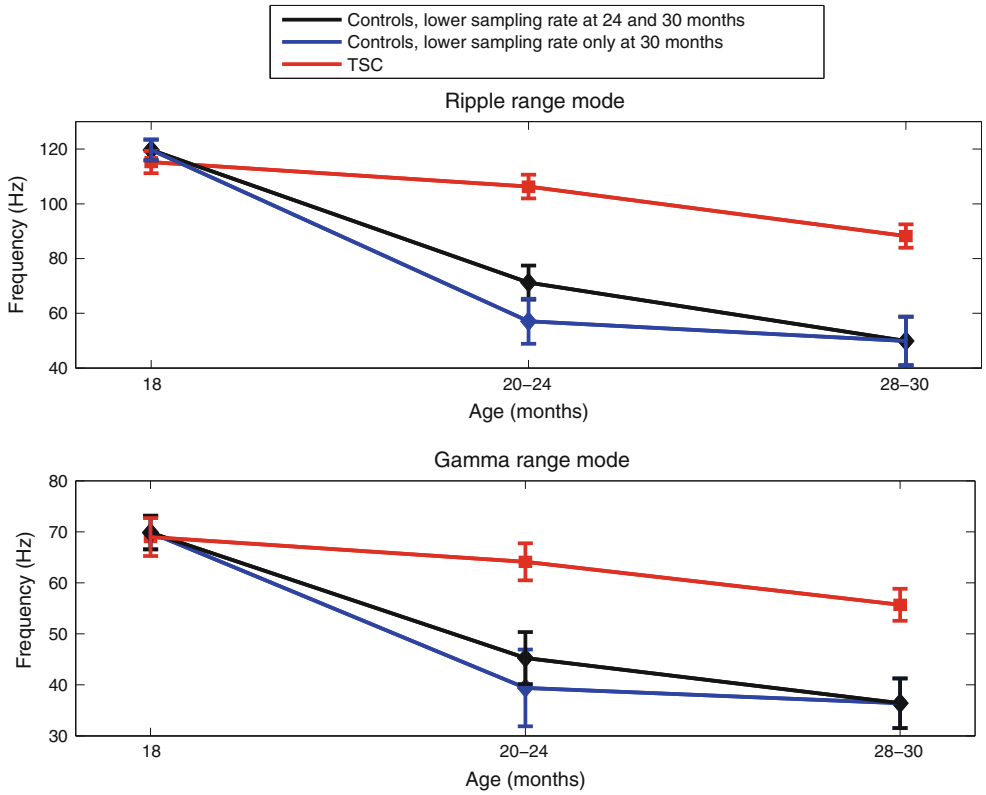

Fig. 11 Ripple and high-gamma frequencies as a function of age during mom trials. Mean frequency, averaged over trials, channels, and subjects and corresponding variability (±1 SD) are superimposed in controls sampled at 250 samples/s at ages ≥20 months (*blue*), controls sampled 500 samples/s at 18 and 24 months (*black*), and TSC subjects (*red*) (Color figure online)

very small samples sizes, but they still suggest that strengthening of neural circuits during development may be encoded in the EEG in part as progressive decrease in spatially distributed low-amplitude, high-frequency activity. High-frequency activity, above (>80 Hz) and/or at the high-gamma range (60–80 Hz) may represent some type of 'neuronal noise', which may decrease with increasing axonal myelination during development and maturation of functional circuits. Recent neuroimaging studies have measured the dynamics of myelination, which occurs at different rates in the brain, but is visible across the brain by age 9 months (Deoni et al. 2011). This process may be delayed in TSC, and increased high-frequency activity at least until 24 months, may reflect a slower overall rate of myelination and maturation of neuronal networks.

Estimated modal frequencies had consistent spatial patterns. High-frequency modes were spatially diffused, with relatively lower spatial specificity to particular brain regions. Localization of individual modes increased with decreasing frequency, i.e., lower frequency modes were typically more highly localized in parietal, temporal and fronto-temporal regions, in both baseline and task-related signals. Significant differences in these patterns were estimated between TSC and healthy infants in the 28–30 month, and to some extent the 20–24 month age range. Visual tasks also modulated modal frequencies. Lower ripple and high-gamma frequencies were estimated in both TSC and controls during stimulus presentation. However, differences between tasks were not statistically significant. In addition, more spatially localized low-gamma frequencies were estimated during presentation of images and checkerboards, but differences in frequencies in this range, were insignificant between task and non-task signals. Distinct spatial patterns of modal frequencies in the alpha and theta ranges were estimated between TSC and healthy infants at 18 months. Higher and more highly localized temporal and fronto-temporal alpha and theta frequencies were estimated in TSC. In contrast, more spatially distributed frequencies were estimated in controls, particularly in frontal and fronto-central regions. This is the opposite than the spatial patterns observed at high frequencies. In older infants, there were no consistent statistically significant differences between TSC and controls for modal frequencies below 30 Hz. In the 20–22 month control subgroup, statistically lower frequencies in the beta to theta ranges were estimated during presentation of mom and stranger images. In the 24 month control subgroup, no significant differences were found. Although the two subgroups were sampled at different rates (250 vs. 500 samples/s), this variability may be due to the small size of the

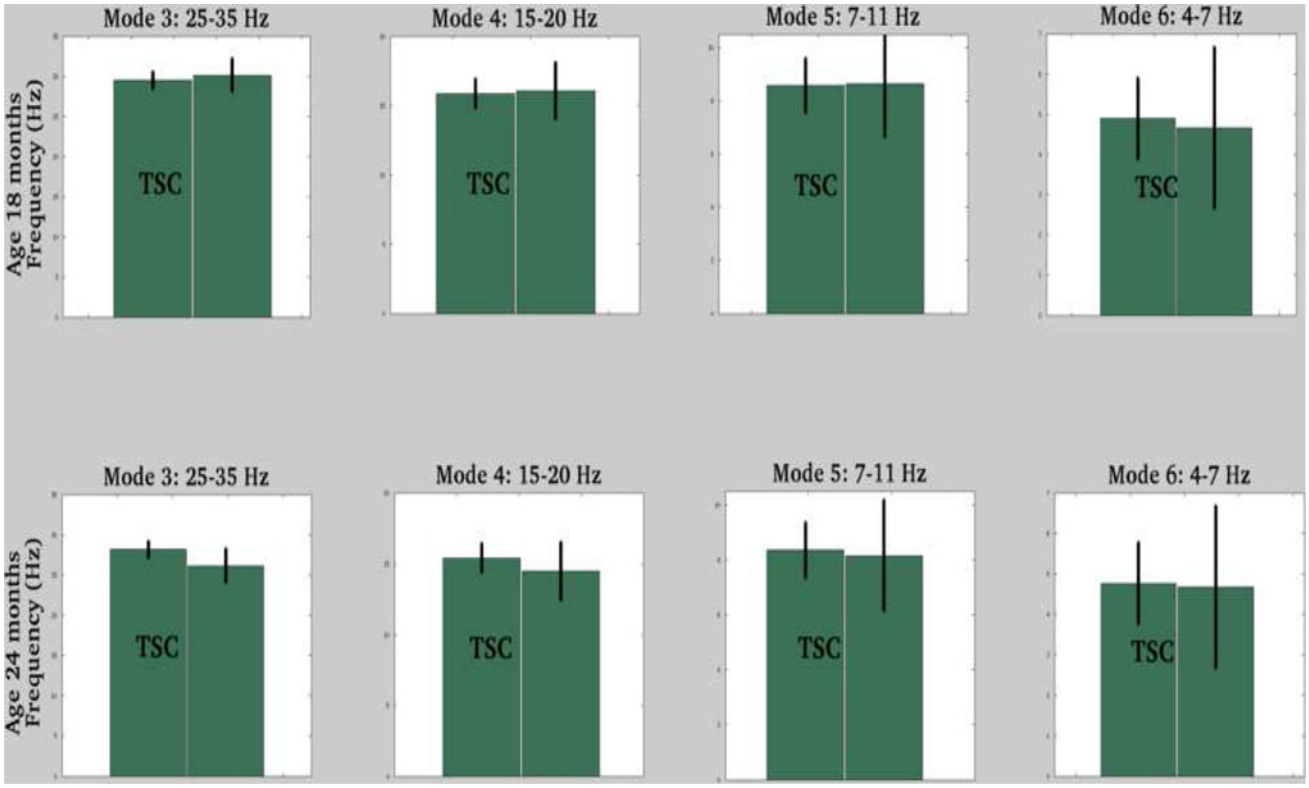

Fig. 12 Mean differences in modal frequencies, in the low-gamma/high-beta, beta, alpha and theta ranges (from *left* to *right*), estimated during presentation of mom images, in healthy and TSC infants at 18 and 24 months

two subgroups (3 subjects), and thus not due to the sampling rate limitation.

Despite promising findings, this study has several limitations. First, the samples were small, which limits the extent of statistical analysis and the robust statistical characterization of differences in estimated parameters. Clearly, the results need to be validated in larger TSC and healthy infant cohorts. In addition, several pairwise comparisons are made, i.e., for individual modes, under different recording conditions, etc. A larger sample may allow the development of statistical models that include multiple parameters for combinatorial prediction of differences in rhythm dynamics between TSC and controls. However, despite the small sample sizes, a significant amount of EEG data were analyzed, from relatively long baseline intervals, different tasks, and multiple trials and segments per task. Results were remarkably consistent under the different experimental conditions, at frequencies above 30 Hz, which in turn suggests that estimated dominant frequencies in this range may represent a stable parameter of brain neurodynamics, which is robust to inter-subject and inter-trial variability. Estimated frequencies at lower ranges ($\leq$30 Hz) were less consistent, at least in the 20–24 month range, with increasing inter-subject variability as frequency decreased. This highlights the need to validate these results in a larger study. Another limitation is that no longitudinal data were included in the analysis, i.e., different subjects were included in each age subgroup. Therefore, it is possible that estimated age effects may be due to intra-group variability. Finally, it is possible that lower modal frequencies at 28–30 months in healthy infants compared to TSC are due to differences in sampling rate than true age-related differences. However, we were able to compare non-task and face trials in two subgroups of healthy controls at 20–24 months, one sampled at 250 samples/s (with a 64-electrode system) and the other at 500 samples/s (with a 128-electrode system). There were no statistically significant differences due to sampling (spatial or temporal) at frequencies in the gamma and ripple ranges, at which the sampling rate limitation could affect the results. Overall, the highest estimated frequency in infants >18 months was on average $\leq$90 Hz. Modal frequencies and amplitudes were averaged over large number of trials. Although beyond the scope of this study, a detailed analysis of inter-trial differences between estimated frequencies may be informative. Finally, there remains a possibility that high-frequency modes represent non-neural noise contributions to the EEG. However, based on extensive filtering followed by decomposition-based denoising of each EEG signal, and careful examination of the auto-correlation functions corresponding to the ripple and high-gamma modes it is unlikely that these modes are associated with non-neural

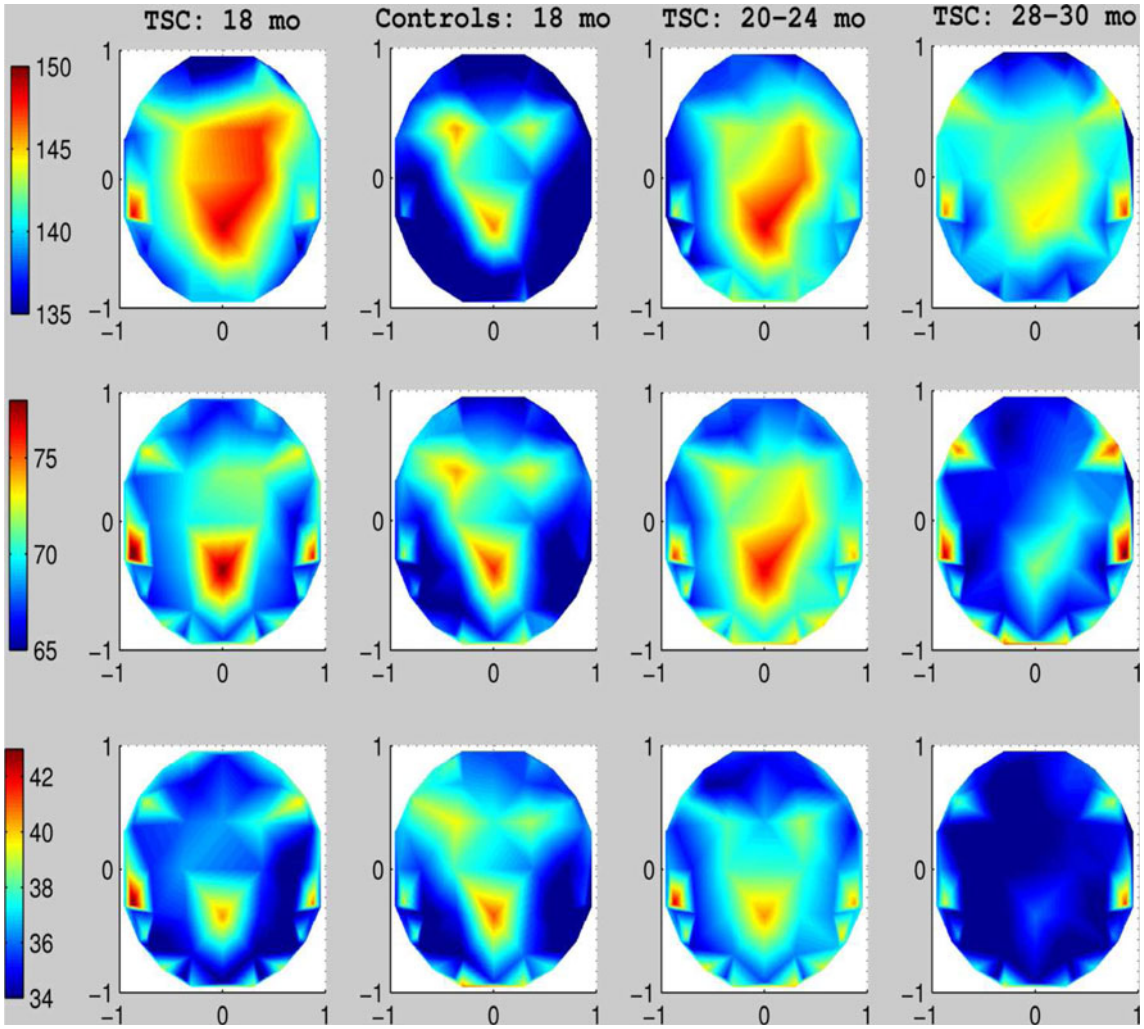

Fig. 13 Spatial distribution of first 3 modal frequencies during checker trials. From *left* to *right panels* TSC, 18 months, Controls 18 months, TSC 20–24 months, and TSC 28–30 months. Ripple (>80 Hz, *top panels*) and gamma modes (*middle* and *bottom panels*) are shown. *Colorbars* correspond to frequency in Hz (Color figure online)

noise. Furthermore, these modes were consistently modulated by stimulus presentation and age.

In summary, this study presents novel findings on the spectral characteristics of neural activity in infants (age 18–30 months) with TSC and age-matched controls, measured by high-density scalp EEG. We have shown that high-frequency, non-noise signal components are measurable in both resting and task-related EEG and are significantly modulated by age, possibly reflecting maturation of developing neural circuits and increased processing efficiency with age. This activity decreases with age, but at a slower rate in TSC than in controls. Although the role of this activity is not yet understood, it may represent a low-amplitude signal induced by noisy neuronal networks. Increased myelination and connection strengthening with age may result in the attenuation of this activity. In turn, this suggests that functional connectivity, which is directly correlated with network integrity, may be impaired in younger infants with TSC even at 20–24 months, resulting in poorer cognitive performance. Therefore, this analysis provides novel insights into specific aspects of neurodynamic development in infants with TSC, which may ultimately improve our understanding of the underlying mechanisms of cognitive deficits in these patients. Finally, consistent detection of differences in the spatio-temporal distribution of modal frequencies at different ages may have important implications for diagnosis, as well as prediction of the cognitive outcome and potentially the risk of comorbid connectivity/information processing disorders such as ASD.

Acknowledgments This study was supported in part by the department of Radiology, Boston Children's Hospital (CS), the Harvard Clinical and Translational Science Center (NIH Award #UL1 RR 025758) (CS), and a Department of Defense grant (W81XWH-10) (CA). The content is solely the responsibility of the authors. We are grateful to the families of participating subjects, as they have made this research possible.

References

Au, K. S., Williams, A. T., Roach, E. S., et al. (2007). Genotype/phenotype correlation in 325 individuals referred for a diagnosis of tuberous sclerosis complex in the United States. *Genetics in Medicine, 9*(2), 88–100.

Bolton, P. F., Park, R. J., Higgins, J. N., et al. (2002). Neuro-epileptic determinants of autism spectrum disorders in tuberous sclerosis complex. *Brain, 125*(Pt6), 1247–1255.

Burgess, A. P. (2012). Towards a unified understanding of event-related changes in the EEG: The firefly model of synchronization through cross-frequency phase modulation. *PLoS One, 7*(9), e45630.

Crino, P. B., Nathanson, K. L., & Henske, E. P. (2006). The tuberous sclerosis complex. *New England Journal of Medicine, 355*, 1345–1356.

Dabora, S. L., Jozwiak, S., Franz, D. N., et al. (2001). Mutational analysis in a cohort of 224 tuberous sclerosis patients indicated increased severity of TSC2, compared with TSC1, disease in multiple organs. *American Society of Human Genetics, 68*(1), 64–80.

D'Argenzio, L., Koch, G., Bombardieri, R., et al. (2009). Abnormal parieto-motor connectivity in tuberous sclerosis complex. *Epilepsy Research, 87*(1), 102-5.

Deoni, S. C., Mercure, E., & Blasi, A. (2011). Mapping infant brain myelination with magnetic resonance imaging. *Journal of Neuroscience, 31*(2), 784–791.

EGI Technical Note (2005). Determination of the Geodesic Sensor Nets average electrode positions and their 10-10 international equivalents, Electrical Geodesics, Inc., Eugene, OR.

Gallagher, A., Chu-Shore, C. J., Montenegro, M. A., et al. (2009). Associations between electroencephalographic and magnetic resonance imaging findings in tuberous sclerosis complex. *Epilepsy Research, 87*(2-3), 197–202.

Geddes, L. A., & Baker, L. E. (1967). The specific resistance of biological material, a compendium of data for the biomedical engineer and physiologist. *Medical and Biological Engineering and Computing, 5*, 271–293.

Guttierez, G. C., Smalley, S. L., & Tanguay, P. E. (1998). Autism in tuberous sclerosis complex. *Journal of Autism and Developmental Disorders, 28*, 97–103.

Harrison, J. E., & Bolton, P. F. (1997). Annotation: Tuberous sclerosis. *Journal of Child Psychology and Psychiatry, 38*(6), 603–614.

Holmes, G. L., & Stafstrom C. E. (2007). Tuberous sclerosis study group, tuberous sclerosis complex and epilepsy: Recent developments and future challenges. *Epilepsia, 48*(4), 617–630.

Huang, N. E., Shen, Z., Long, S. R., et al. (1998). Empirical Mode Decomposition and Hilbert spectrum for non-linear, non-stationary time series analysis. *Proceedings of the Royal Society of London, Series A: Mathematical and Physical Sciences, 454*, 903–995.

Irahara, K., Nakagawa, E., Honda, R., et al. (2012). High gamma activity of 60–70 Hz in the area surrounding a cortical tuber in an infant with tuberous sclerosis. *Italian Journal of Pediatrics, 38*, 15.

Jacobs, J., Rohr, A., Moeller, F., et al. (2008). Evaluation of epileptogenic networks in children with tuberous sclerosis complex using EEG-fMRI. *Epilepsia, 49*(5), 816–825.

Jansen, F. E., Braams, O., Vincken, K. L., et al. (2008). Overlapping neurologic and cognitive phenotypes in patients with TSC1 and TSC2 mutations. *Neurology 70*(12), 908–915.

Jeste, S. S., Sahin, M., Bolton, P. et al. (2008). Characterization of autism in young children with tuberous sclerosis complex. *Journal of Child Neurology, 23*(5), 520–525.

Kandt, R. S., Haines, J. L., Smith, M. et al. (1992). Linkage of an important gene locus for tuberous sclerosis to a chromosome 16 marker for polycystic kidney disease. *Nature Genetics*, 237–241.

Kleinhans, N. M., Richards, T., Sterling, L., et al. (2008). Abnormal functional connectivity in autism spectrum disorders during face processing. *Brain, 131*, 1000–1012.

Major, P., Rakowski, S., Simon, M. V., et al. (2009). Are cortical tubers epileptogenic? Evidence from electrocorticography. *Epilepsia, 50*(1), 147–54.

Markel, J. D. (1972). The SIFT algorithm for fundamental frequency estimation. *IEEE Transactions on Audio and Electroacoustics, 20*, 367–377.

McGrath, J., Johnson, K., Ecker, C., et al. (2012). Atypical visuospatial processing in autism: Insights from functional connectivity analysis. *Autism Research, 5*(5), 314–30.

Muzykewicz, D. A., Newberry, P., Danforth, N., et al. (2007). Psychiatric comorbid conditions in a clinic population of 241 patients with tuberous sclerosis complex. *Epilepsy and Behavior, 11*, 506–513.

Nebel, M. B., Joel, S. E., Muschelli, J., et al. (2012). Disruption of functional organization within the primary motor cortex in children with autism, *Human Brain Mapping* (Epub ahead of press).

Numis, A. L., Major, P., Montenegro, M. A., et al. (2011). Identification of risk factors for autism spectrum disorders in tuberous sclerosis complex. *Neurology, 76*(11), 981–987.

Oostendorp, T. F., Delbecke, J., Stegeman, D. F. (2000). The conductivity of the human skull: Results of in vivo and in vitro measurements. *IEEE Transactions on Biomedical Engineering, 47*, 1487–1492.

Peters, J. M., Sahin, M., Vogel-Farley, V. K., et al. (2012). Loss of white matter micro-structural integrity is associated with adverse neurological outcome in tuberous sclerosis complex. *Academic Radiology, 19*(1), 17–25.

Phadke, A., Thorp, J., & Adamiak, M. (1983). A new measurement technique for tracking voltage phasors, local systems frequency, and rate of change of frequency. *IEEE Transaction on Power Applications System, PAS-102*, 1025–1038.

Shepherd, C. W., & Stephenson, J. B. P. (1992). Seizures and intellectual disability associated with tuberous sclerosis complex in the West of Scotland. *Developmental Medicine and Child Neurology, 34*, 766–774.

Stamoulis, C., & Chang, B. S. (2009). Application of matched-filtering to extract EEG features and decouple signal contributions from multiple seizure foci in brain malformations. In *IEEE Proceedings of the 4th International IEEE/EBMS Conference on Neural Engineering*, (pp. 514–517).

Stamoulis, C., & Betensky, R. A. (2011). A novel signal processing approach for the detection of copy number variations in the human genome. *Bioinformatics, 27*(17), 2338–2345.

Sweeney, K., McLoone, S., & Ward, T. (2012). The use of ensemble empirical mode decomposition with canonical correlation analysis as a novel artifact removal technique, *IEEE Transactions on Biomedical Engineering* (Epub ahead of print).

Sweeney-Reed, C. M., & Nasuto, S. J. (2009). Detection of neural correlates of self-paced motor activity using empirical model decomposition phase locking analysis. *Journal of Neuroscience Methods, 184*(1), 54–70.

Tsai, P. H., Lin, C., Tsao, J., et al. (2012). Empirical mode decomposition based detrended sample entropy in electroencephalography for Alzheimer's disease. *Journal of Neuroscience Methods, 210*(2), 230–237.

Thomson, D. J. (1982). Spectrum estimation and harmonic analysis. *Proceedings of the IEEE, 70*, 1055–1096.

Van Slegtenhorst, M., De Hoogt, R., Hermans, C., et al. (1997). Identification of the Tuberous Sclerosis gene TSC1 on chromosome 9q34. *Science, 277*(5327), 805–808.

Webb, D. W., Fryer, A. E., & Osborne, J. P. (1991). On the incidence of fits and mental retardation in tuberous sclerosis. *Journal of Medical Genetics, 28*, 395–397.

Wu, Z., & Huang, N. E. (2004). A study of the characteristics of white noise using the empirical model decomposition method. *Proceedings of the Royal Society of London, 460*, 1597–1611.